Strain-induced phase transformations under compression, unloading, and reloading in a diamond anvil cell

Biao Feng, Oleg M. Zarechnyy, and Valery I. Levitas

Citation: Journal of Applied Physics **113**, 173514 (2013); doi: 10.1063/1.4803851
View online: http://dx.doi.org/10.1063/1.4803851
View Table of Contents: http://scitation.aip.org/content/aip/journal/jap/113/17?ver=pdfcov
Published by the AIP Publishing

Strain-induced phase transformations under compression, unloading, and reloading in a diamond anvil cell

Biao Feng,[1] Oleg M. Zarechnyy,[1] and Valery I. Levitas[2,a)]
[1]*Department of Aerospace Engineering, Iowa State University, Ames, Iowa 50011, USA*
[2]*Departments of Aerospace Engineering, Mechanical Engineering, and Material Science and Engineering, Iowa State University, Ames, Iowa 50011, USA*

(Received 28 February 2013; accepted 15 April 2013; published online 7 May 2013)

Strain-induced phase transformations (PTs) in a sample under compression, unloading, and reloading in a diamond anvil cell are investigated in detail, by applying finite element method. In contrast to previous studies, the kinetic equation includes the pressure range in which both direct and reverse PTs occur simultaneously. Results are compared to the case when "no transformation" region in the pressure range exists instead, for various values of the kinetic parameters and ratios of the yield strengths of low and high pressure phases. Under unloading (which has never been studied before), surprising plastic flow and reverse PT are found, which were neglected in experiments and change interpretation of experimental results. They are caused both by heterogeneous stress redistribution and transformation-induced plasticity. After reloading, the reverse PT continues followed by intense direct PT. However, PT is less pronounced than after initial compression and geometry of transformed zone changes. In particular, a localized transformed band of a weaker high pressure phase does not reappear in comparison with the initial compression. A number of experimental phenomena are reproduced and interpreted. [http://dx.doi.org/10.1063/1.4803851]

I. INTRODUCTION

A diamond anvil cell is a powerful tool to generate high pressure and *in situ* study phase transformation (PTs) to high pressure phases, using modern diagnostics, like x-ray, Raman, and optical techniques.[1–5] When hydrostatic media is used, PT is classified as pressure-induced one and it starts by nucleation at pre-existing defects (pressure and stress concentrators). In order to study the effect of plastic deformations on PTs, a rotational diamond anvil cell (DAC) was utilized,[6–10] in which large plastic shear due to rotation of one of the anvils is superposed on high pressure. Such PTs are classified as strain-induced ones and they occur by nucleation at defects that continuously appear during the plastic deformation.[11] In fact, PTs under compression without hydrostatic media in traditional DAC are also strain-induced rather than pressure-induced, because they occur during intense plastic flow of materials.[11,12] As it was discussed in Refs. 11–13, the only difference between PTs under compression in DAC and compression and torsion in rotational DAC is the pressure-plastic strain history for each material point of the sample. It was found in Refs. 11, 14, and 15 that strain-induced PTs require completely different thermodynamic and kinetic treatment and experimental characterization than pressure-induced PTs. Thus, the main focus is on the strain-controlled kinetic Eq. (8) for the concentration of the high pressure phase, c, with respect to undeformed state, which is independent of time and depends on four main parameters: (1) kinetic parameter k which scales the rate of PTs, (2) the minimum pressure p_ε^d below which direct strain-induced PT cannot occur, (3) the maximum pressure p_ε^r above which reverse strain-induced PT does not take place, and (4) the ratio of yield strengths of low (σ_{y1}) and high pressure (σ_{y2}) phases. We are unaware of any publications that determine parameters of the kinetic equation and fields of stress and strain tensors experimentally. Pressure distribution[8,16–20] and concentration of high pressure phase distributions[18,19] along the radius of a sample are available only. As a consequence, theoretical and finite element methods have been developed and applied for investigation of variation of stress tensor, accumulated plastic strain, and concentration fields in a sample during plastic flow and PTs and for analysis and interpretation of experimental results.[11–13,21,22] Numerical results, published in Refs. 12, 13, 21, and 22, describe a number of experimental observations, however they are incomplete because they are obtained for $p_\varepsilon^d > p_\varepsilon^r$ only. In this case, both direct and reverse PTs cannot occur for values of pressure p in the range $p_\varepsilon^r < p < p_\varepsilon^d$; above p_ε^d, direct PT occurs only and below p_ε^r, reverse PT takes place only, reaching complete transformation at very large plastic strain. However, the case $p_\varepsilon^d < p_\varepsilon^r$ is at least of the same importance, for which both direct and reverse PTs occur in the pressure range $p_\varepsilon^d < p < p_\varepsilon^r$. This leads to a stationary value of concentration $0 < c < 1$ at very large plastic strains, which was observed experimentally for various pressure-shear loading, e.g., under high pressure torsion[23–25] and ball milling.[26–29] Therefore, new PT features and phenomena may appear. One of the *goals* of the paper is to study in detail coupled plastic flow and PTs in a sample in DAC for the case with- and various values of the kinetic parameter k and the ratio of the yield strengths, and to compare results with the case of $p_\varepsilon^d > p_\varepsilon^r$. Another *goal* is to study plastic flow and PTs after

a)Author to whom correspondence should be addressed. Electronic mail: vlevitas@iastate.edu

unloading and *reloading*, which was never done before. In many cases, high pressure phase is metastable after pressure release and can exist and be studied at ambient conditions. However, if there is no reverse PT under hydrostatic loading-unloading, this does not mean that reverse PT will not occur during the reduction of the load to zero after strain-induced PT. In many cases (excluding in situ studies), concentration of phases is determined after unloading[23–29] but is related to the loading process with a salient assumption that it does not change during unloading because of the absence of plastic deformation. As we will show, in contrast, unloading is accompanied in many cases by plastic flow and reverse PT, which should be taken into account in experiments. Finally, reloading is studied to explore an additional pressure-plastic strain path and its relevance for experimental realization.

II. PROBLEM FORMULATION

Phase transformations coupled to plastic flow, in a sample of radius $\tilde{R}$ compressed by axial force P between two rigid diamonds under loading, unloading, and reloading are studied in this paper using the same physical and geometric models as in Refs. 12, 13, and 22. Geometry and boundary conditions are shown in Fig. 1.

To obtain generic results, we consider the simplest isotropic, perfectly plastic model, and the total system of equations are given as follows:[12]

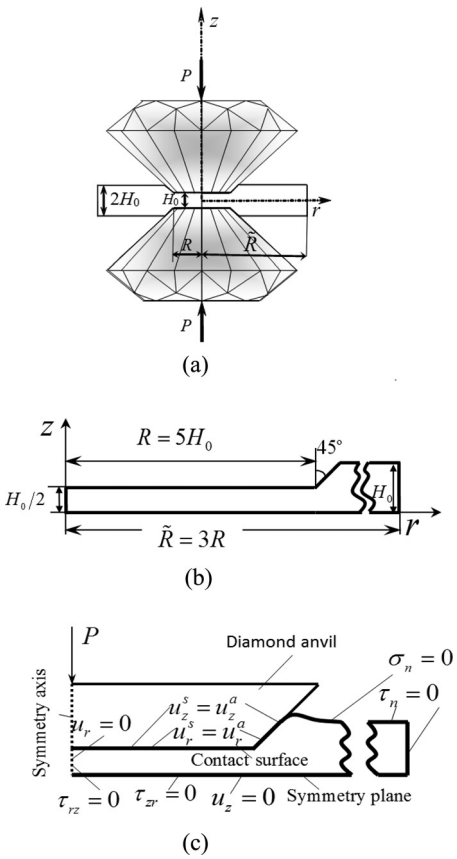

FIG. 1. (a) Diamond anvil cell scheme, (b) quarter of a sample in initial undeformed state, and (c) boundary conditions including no slipping on the contact surface between sample and diamond anvil.

Decomposition of deformation rate $\mathbf{d}$ into elastic (subscript e), transformational (t), and plastic (p) contributions

$$\mathbf{d} = \overset{\nabla}{\varepsilon}_e + \dot{\varepsilon}_t \mathbf{I} + \mathbf{d}_p. \tag{1}$$

Elasticity rule (Hooke's law)

$$p = K\varepsilon_{e0}; \quad \mathbf{s} = 2G\, dev\boldsymbol{\varepsilon}_e. \tag{2}$$

Transformation volumetric strain

$$\varepsilon_t = \bar{\varepsilon}_t c. \tag{3}$$

Von Mises yield condition

$$\sigma_i = \left(\frac{3}{2}\mathbf{s}:\mathbf{s}\right)^{0.5} \le \sigma_y(c) = (1-c)\sigma_{y1} + c\sigma_{y2}. \tag{4}$$

Plastic flow rule in the plastic region

$$\sigma_i = \sigma_y(c) \text{ and } \mathbf{s}\cdot\dot{\mathbf{s}} > 0 \rightarrow \mathbf{d}_p = \lambda\mathbf{s},$$
$$\lambda = \frac{3}{2}\frac{\mathbf{s}:\mathbf{d}}{\sigma_y^2} - \frac{\dot{c}(\sigma_{y2}-\sigma_{y1})}{\sigma_y G}, \tag{5}$$

in the elastic region

$$\sigma_i < \sigma_y(c) \quad \text{or} \quad \sigma_i = \sigma_y(c) \quad \text{and} \quad \mathbf{s}\cdot\dot{\mathbf{s}} \le 0 \rightarrow \mathbf{d}_p = 0. \tag{6}$$

Momentum balance equation

$$\nabla\cdot\mathbf{T} = 0. \tag{7}$$

Strain-controlled kinetics for phase transformations

$$\frac{dc}{dq} = 10k\frac{(1-c)\bar{p}_d H(\bar{p}_d)\frac{\sigma_{y2}}{\sigma_{y1}} - c\bar{p}_r H(\bar{p}_r)}{c + (1-c)\sigma_{y2}/\sigma_{y1}} \tag{8}$$

with $\dot{q} = (2/3\mathbf{d}_p:\mathbf{d}_p)^{1/2}$, $\bar{p}_d = \frac{p-p_\varepsilon^d}{p_h^d - p_\varepsilon^d}$, and $\bar{p}_r = \frac{p-p_\varepsilon^r}{p_h^r - p_\varepsilon^r}$.

Here, $\mathbf{s}$ is the deviator of the true stress tensor $\mathbf{T}$, $\mathbf{s} = dev\mathbf{T}$; $\overset{\nabla}{\varepsilon}_e$ and $\overset{\nabla}{\mathbf{s}}$ are the Jaumann objective time derivative of the elastic strain and deviatoric stress; $\mathbf{I}$ is the second-rank unit tensor; K and G designate bulk and shear moduli, respectively; σ_i is the second invariant of the stress deviator; ε_{e0} and $\bar{\varepsilon}_t$ are the elastic and transformation volumetric strains for complete PT, respectively; H is the Heaviside step function; p_h^d and p_h^r are the pressures for direct and reverse PTs under hydrostatic loading, respectively, and $q$is the accumulated plastic strain (Odqvist parameter). Without PTs, the applicability of the perfectly plastic and isotropic model for monotonous loading is justified in Ref. 30 for various classes of materials (rocks, metals, pressed powders, etc.) starting with plastic strains $q > 0.6 \div 1$ both for normal and high pressure. Additional confirmations for steel and NaCl were obtained with rotational DAC in Ref. 31. Note that the yield strength in the perfectly plastic state is independent of the deformation history.[30] Also, our goal is to perform simulation of *strain-induced* PTs rather

than just plastic flow. Since there is no available experimental data on such transformations, there is no sense to combine more sophisticated models for plastic straining (e.g., model for a polycrystalline aggregate[32]) with the simplest model for PT.

Assumption of small elastic strains limits pressure to the value of 0.1 K, which is of the order of magnitude of 10 GPa. Under such a maximum pressure, change in geometry of the diamond anvils is negligible, which can be shown by solution of elastic problem for an anvil.[33–35] Thus, assumption that the anvils are rigid is justified.

It is not a problem to include deformation of anvils and strain hardening in the model, if it would be necessary. However, this paper is among very few first numerical studies of *strain-induced* PTs in DAC and as we wrote before, we want to obtain results that are generic for a wide class of materials. If we introduce some hardening parameters and/or specific geometry of an anvil and way of its fixation, we will lose the generic character of the results and gain the secondary effects only.

Finite element method and code ABAQUS[36] have been utilized for solution of axial symmetric problems. In the dimensionless form, all stress related parameters (excluding shear stress, see below) are divided by σ_{y1}; the dimensionless axial force F normalized by the product of total initial contact area of a sample and σ_{y1}. For precise comparison with the results for $p_\varepsilon^d > p_\varepsilon^r$ in Ref. 22, we assume dimensionless $h/2$ and σ_n=0 (i.e., just switch values $p_\varepsilon^d = 6.75$ and $p_\varepsilon^r = 6.375$) and keep other material parameters, $p_h^d = 11.25$ and $p_h^r = 1.875$ exactly the same like in Ref. 22.

III. PHASE TRANSFORMATIONS UNDER LOADING

In this section, our principal aim is to investigate effects of characteristic pressures for $p_\varepsilon^d < p_\varepsilon^r$ (in contrast to Ref. 22) on PTs, for various kinetic parameters k and ratios of yield strengths of high and low pressure phases. Previous simulations[12,13,21,22] with $p_\varepsilon^d > p_\varepsilon^r$ did not allow the PTs to occur when pressure p lies between two characteristic pressures, $p_\varepsilon^r < p < p_\varepsilon^d$. In the current simulations, $p_\varepsilon^d < p_\varepsilon^r$ and therefore there is no such limitation, and both direct and reverse PTs can happen when $p_\varepsilon^d < p < p_\varepsilon^r$. Before high pressure phase appears, the largest pressure is located at the center of a sample, and pressure is gradually decreasing with increase of coordinates r or z. Once pressure reaches p_ε^d at the center of sample and since accumulated plastic strain increases in most region of $r \le R$, high pressure phase first appears there, regardless of the value of k and the ratio of yield strengths. However, close to p_ε^d concentration of high pressure phase is still pretty low and is not shown in Fig. 2.

Concentration of a weaker ($\sigma_{y2} = 0.2\sigma_{y1}$) high pressure phase c is shown in Fig. 2 with $k = 5, 10, 30$ and under the rising dimensionless load F. One can note that: (1) with load F rising, PT shifts from the center to a localized plastic shear and PT bands and then propagates within these bands; (2) geometry of the transformed zone differs from the case with $p_\varepsilon^d > p_\varepsilon^r$,[12,13,21,22] especially for $k = 5$, when the multi-connected transformed region first appears due to strain localization and heterogeneous pressure distribution; and (3)

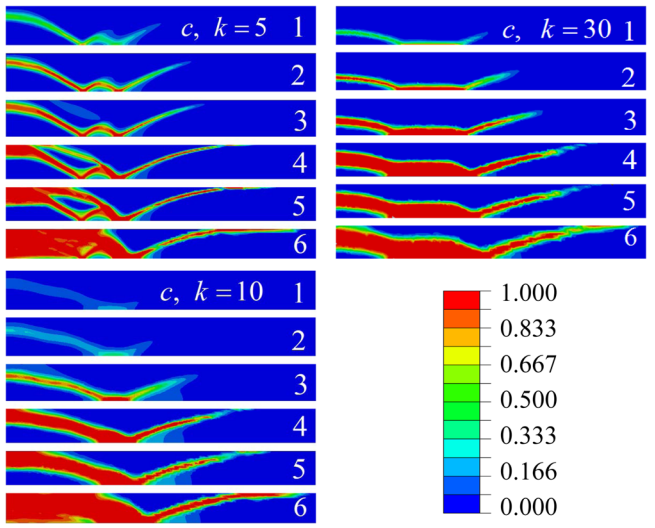

FIG. 2. Concentration of high pressure phase c under loading for $k = 5$, 10, and 30; $\sigma_{y2} = 0.2\sigma_{y1}$ and $r/R \le 0.72$ in Fig. 1(b). The dimensionless axial force F is (1) 4.09, (2) 4.23, (3) 4.37, (4) 4.54, (5) 4.71, and (6) 4.97.

in contrast Ref. 22, PTs for all k reach the contact surface at lower load, which is convenient for detecting PTs using surface-based (e.g., optical and Raman) methods in experiments; especially for $k = 30$ PTs in Ref. 22 did not reach the surface at all. Because the threshold value p_ε^d for direct PT is accepted lower in this paper than that in Ref. 22, direct PT occurs at lower load in the region close to contact surface, where the pressure is usually lower than the one at the symmetry plane at the same coordinate$r$.

Fig. 3 shows the distributions of pressure p and the volume fraction of a weaker high pressure phase c at the contact surface of the sample for k equal to 5 and 10. There are two separate regions where PT occurs, and two pressure plateaus appear there with pressures well above p_ε^d and p_ε^r. Between two PT regions, another plateau in pressure distribution exists with the magnitude between p_ε^d and p_ε^r. However, concentration c in this region is quite low and even equal to zero because of low accumulated plastic strain increment. Also, both direct and reverse PTs occur in this range and even the maximum (stationary) value of c is quite low for the weaker high pressure phase.[14,37] Pressure at the plateau close to the symmetry axis is almost constant under different loads at $k = 5$; pressure at other two plateaus is almost independent of load at $k = 10$. Consequently, the kinetic parameter k not only influences the rate of PT and configuration of PT regions (see Fig. 2) but also determines the positions of constant pressures. In contrast to the case with $p_\varepsilon^d > p_\varepsilon^r$,[22] where the pressure in the weakly or non-transformed region corresponded to p_ε^d, here it is between p_ε^d and p_ε^r. Thus, none of the plateaus correspond to p_ε^d and p_ε^r, and they are determined by mechanics of interaction of plastic flow and PT kinetics. In addition, Fig. 3 exhibits similar oscillatory features of experimental plots for ZnSe[17] and simulation results.[22]

In the rest of this section, PTs to high pressure phase with $\sigma_{y2} \ge \sigma_{y1}$ are discussed. Small steps (plateaus) with almost constant pressure are found in experiments[8,16,17,31] at the very heterogeneous pressure distribution plots. They

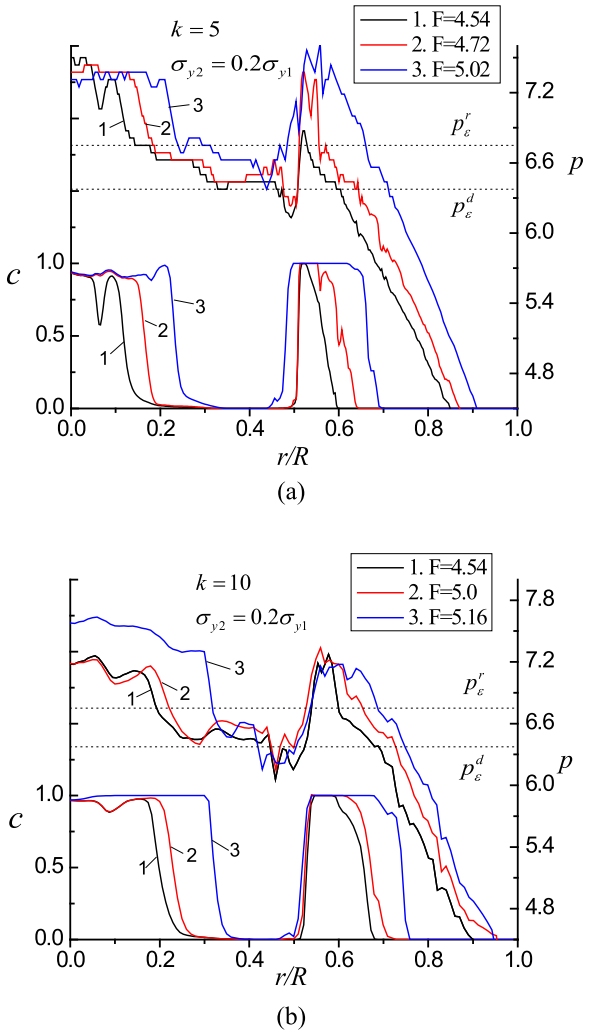

FIG. 3. Distributions of dimensionless pressure p and high pressure phase concentration c on contact surface under loading, for $k = 5$, 10, and $\sigma_{y2} = 0.2\sigma_{y1}$.

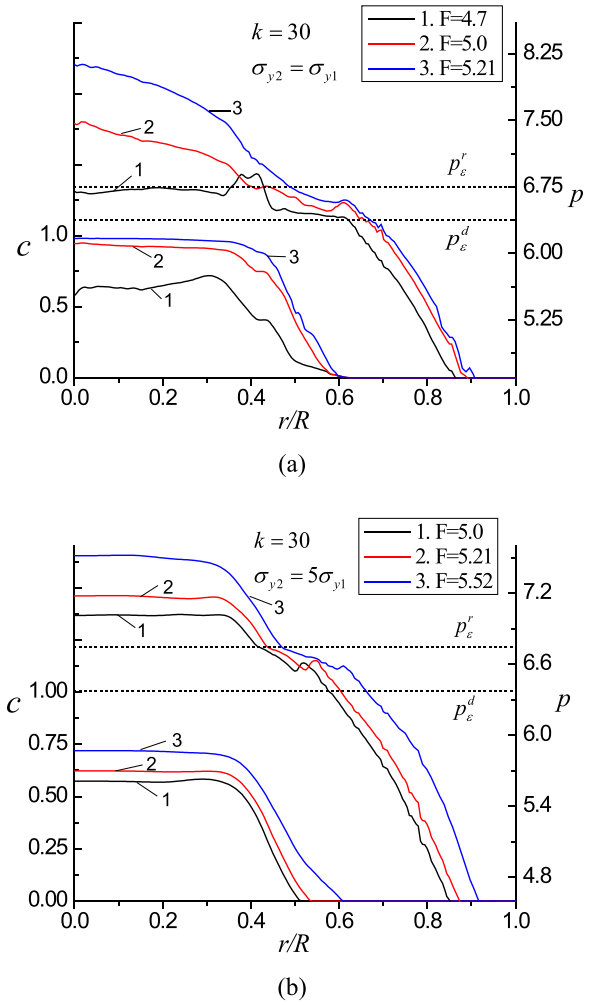

FIG. 4. Distributions of dimensionless pressure p and high pressure phase concentration c on contact surface under loading, for $k = 30$ and $\sigma_{y2} \geq \sigma_{y1}$.

correspond to the two-phase region, which, like in Ref. 22, is clearly reproduced for $k = 30$ only rather than for $k = 1$, 5, or 10. Therefore, for brevity, the concentrations of high pressure phase and pressures on the contact surface are discussed for $k = 30$ only.

Fig. 4 exhibits the same trends as in the experiments in Ref. 17: pressure monotonously grows from the periphery to center; there are two steps in pressure; the first one located in the center of the sample is much wider than the second one, which is located in the two-phase region. Comparing to the case for $\sigma_{y2} = 0.2\sigma_{y1}$ (Fig. 2), the PT localization and pressure oscillations are almost eliminated. Therefore, one wider region instead of two isolated regions with high pressure phase appears on the contact surface of the sample.

While in Ref. 22, pressure at the step in the two-phase region was independent of the load and just slightly above p_ε^d, here it varies between two characteristic pressures p_ε^d and p_ε^r, and increases with increasing load. Thus, it is more difficult to determine the value p_ε^d from experiment for $p_\varepsilon^d < p_\varepsilon^r$ than for $p_\varepsilon^d > p_\varepsilon^r$. Plateaus in the central region of the sample, while similar to those in experiments,[16,31] are not related to p_ε^d and p_ε^r at all.

Fig. 5 shows the distribution of contact shear (friction) stress normalized by the yield strength in shear $\tau_{y1} = \sigma_{y1}/\sqrt{3}$ for $k = 30$ and $\sigma_{y2} \geq \sigma_{y1}$. We accept that the positive direction of shear stress points to the center and corresponds to the flow toward periphery. Due to compression, the material flows from the center to periphery. On the contrary, volumetric reduction due to PT at the center causes the material to flow from periphery to the center in the initial stage of PTs. With further compression, PT has almost completed in the center of the sample and mostly propagated into the two-phase region close to periphery, and then PT causes the material to flow toward this two-phase region instead of the sample's center. Both the direction and magnitude of shear stress on the contact surface result from the competition between these two flows. Because of the symmetry, shear stress is equal to zero at the axis of symmetry; at the periphery $0.7 < r/R < 1$, shear stress is equal to yield strength in shear τ_{y1}. Fig. 5(a) shows that: (1) at the initial stage of PTs at $F = 4.44$, shear stress close to the center is near to zero because both flows due to compression and volume reduction due to PT are small and compensate each other; (2) under further compression, because the flow due to PTs in the center surpasses the flow due to compression, the shear stress becomes negative but then changes sign, and increases until

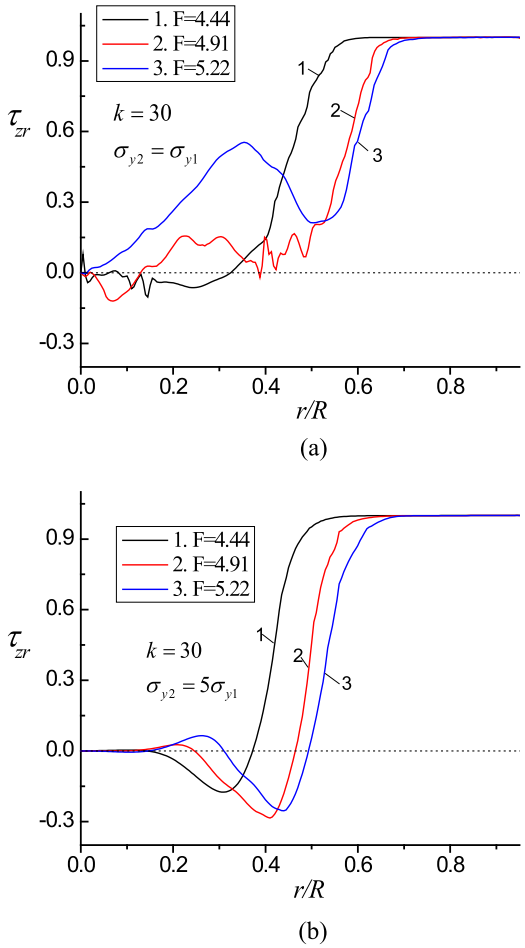

FIG. 5. Distributions of dimensionless pressure τ_{zr} normalized by yield strength in shear τ_{y1} on contact surface under loading, for $k = 30$ and $\sigma_{y2} \geq \sigma_{y1}$.

it reaches the yield shear strength; (3) At $F = 5.22$, the PT at the center is fully completed (therefore, no further reduction in volume is possible) and flow to the periphery due to compression dominates, which causes shear stress to increase from zero to a maximum followed by a drop due to fast PT-induced reduction in volume in two-phase region. Similarly, one could interpret the plots in Fig. 5(b). Like pressure in Fig. 4, the shear stress curve also becomes smoother due to the increase in strength of high pressure phase. Comparison with Ref. 22 demonstrates the similar trends in shear stress, but with some quantitative differences. In particular, the extrema in two-phase region are closer to periphery in our simulations because PTs propagates faster towards periphery due to lower p_ε^d.

IV. STRAIN-INDUCED PHASE TRANSFORMATIONS DURING UNLOADING

Change in concentration of high pressure phase during reduction of applied force down to zero was never studied numerically or in experiments. Characterization of PT processes under pressure based on the results of measurements after complete pressure release[23–29] is based on the strong assumption that there are no PTs during unloading. In this section, the unloading is studied and a surprising result is obtained: for a fast kinetics, $k = 30$, and $\sigma_{y2} \leq \sigma_{y1}$, unloading is accompanied by plastic flow, which causes first a small increase in c above p_ε^d followed by much stronger reverse PT below p_ε^r. We will focus on $k = 30$, because for $k = 10$ and smaller, the change in concentration during unloading is small.

Fig. 6 exhibits variation of concentration c during unloading for three ratios of the yield strengths. Fig. 7 shows distributions of pressure, concentration of the high pressure phase, and accumulated plastic strain along the symmetry plane. The symmetry plane is chosen for comparing with results of reloading, because PTs do not occur on the contact surface under reloading but occur at the symmetry plane (see Sec. V). For $\sigma_{y2} = 5\sigma_{y1}$, PT is not visible under unloading, because the high pressure phase with large yield strength practically does not deform. For $\sigma_{y2} \leq \sigma_{y1}$, significant reduction in concentration, down to complete reverse PTs in some regions is clearly shown. In particular, for the case with $\sigma_{y2} = 0.2\sigma_{y1}$, the transformed band disappears completely.

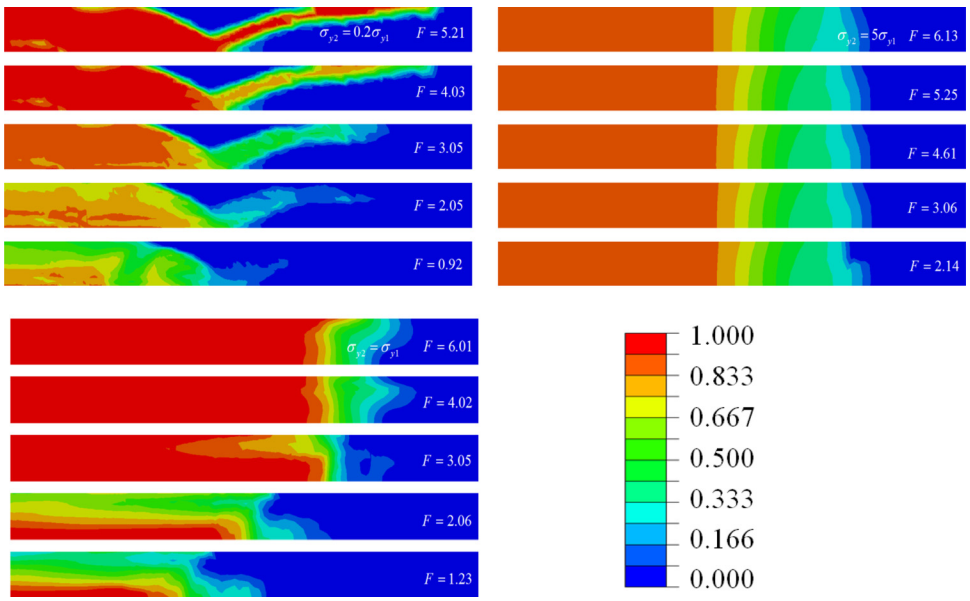

FIG. 6. Concentration of high pressure phase c under unloading for k = 30 and $r/R \leq 0.84$. Initial axial force F for unloading is 5.21 for $\sigma_{y2} = 0.2\sigma_{y1}$, 6.01 for $\sigma_{y2} \geq \sigma_{y1}$, and 6.13 for $\sigma_{y2} = 5\sigma_{y1}$, respectively.

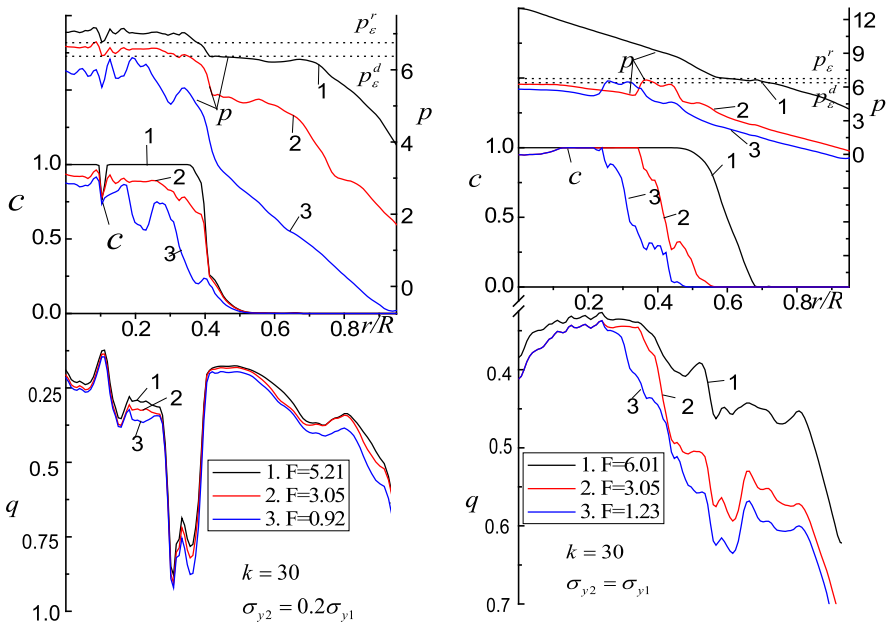

(a) (b)

FIG. 7. Distributions of accumulated plastic strain q, pressure p, and high pressure phase concentration c on symmetry plane under unloading, for $k = 30$ and $\sigma_{y2} \geq \sigma_{y1}$.

Unlike the evolution of the direct PT under loading, reverse PT on unloading progresses from contact surface to symmetry plane and from periphery to center, where pressure is below p_ε^r (see Fig. 7). After almost complete unloading, the high pressure phase mostly retains in the region close to the center and symmetry plane.

It is clear that the reverse PT occurs in the regions where pressure drops below p_ε^r and where plastic straining occurs. For the case $\sigma_{y2} = 0.2\sigma_{y1}$, plastic strain localizes in the weaker high pressure phase, which promotes the reverse PT as soon as p is getting below p_ε^r (Fig. 7(a)). Pressure significantly reduces in the peripheral low pressure phase region of the sample and much smaller reduction is in the central high pressure phase or two phase regions. Plastic strain increment reaches 0.1–0.13 and caused reduction in concentration Δc by up to 0.8. For $\sigma_{y2} = \sigma_{y1}$, the increment of accumulated plastic strain on the symmetry plane in the central region ($r < 0.2R$) appears in the initial stage of unloading only when the pressure is above p_ε^r; at the later stage, there is no change in plastic strain, which results in almost negligible reverse PT (see Figs. 6 and 7(b)). In the region $0.3 < r < 0.7$, plastic strain increment is in the range 0.1–0.25, which in combination with low pressure leads to very intense reverse PT, including complete reverse PT for $r > 0.47$. We would like also to notice that at the very initial stage of unloading, in the region where $p > p_\varepsilon^d$, a small increase in concentration (i.e., direct PT) is observed. This is visible when distributions of c are compared (Fig. 6) in the central region at $F = 5.21$ and $F = 4.03$.

Similar to the pressure distribution on the contact surface, pressure distribution curves on the symmetry plane show steps some of which are in the two-phase region. With the reduction of load, these steps move from the periphery towards the center along with moving two-phase region.

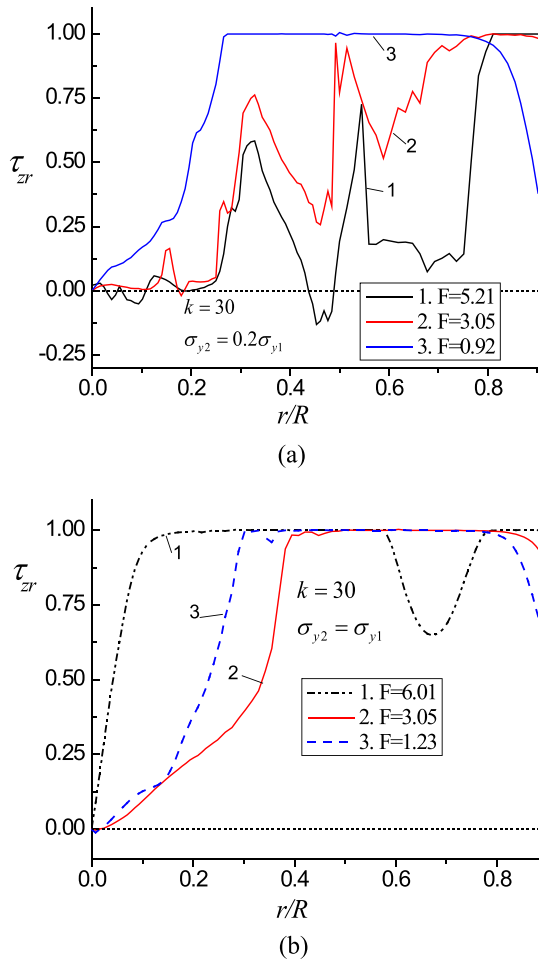

(a)

(b)

FIG. 8. Distribution of dimensionless shear stress τ_{zr} on contact surface under unloading, for $k = 30$ and $\sigma_{y2} \geq \sigma_{y1}$.

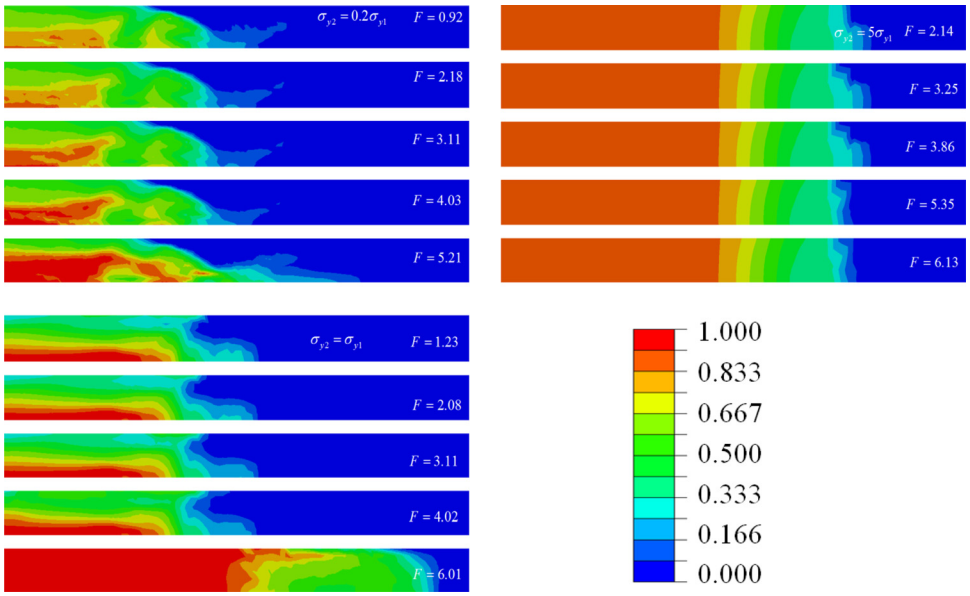

FIG. 9. Concentration of high pressure phase c under reloading for $k = 30$ and $r/R = 0.84$. Initial axial force for reloading Fare, respectively, 0.92 for $\sigma_{y2} = 0.2\sigma_{y1}$, 1.23 for $\sigma_{y2} \geq \sigma_{y1}$, and 2.14 $\sigma_{y2} = 5\sigma_{y1}$.

Localization of PTs and strains determines the irregular distribution of shear stress in Fig. 8(a). Before unloading, there are three drops in shear stress due to heterogeneous reduction in volume during PT and plastic flow. Under unloading, Fig. 8(a) shows that the rise in shear stress due to increase in volume during the reverse PT surpasses the reduction of shear stress due to unloading. Shear stress reaches the yield strength in shear in the major part of the contact surface. For the case $\sigma_{y2} = \sigma_{y1}$ in Fig. 8(b), the initial stage of unloading, reverse PT mostly occurs in the two-phase region rather than at center (see Fig. 6). This causes shear stress increase in the two-phase region and decrease at the center due to reduction of loading. At further unloading, the reverse PT shifts to the center, which results the increase of shear stress in the center.

To summarize, for fast kinetics ($k = 30$) and $\sigma_{y2} \leq \sigma_{y1}$, unloading causes plastic flow, which first induces a small increase in c above p_ε^d followed by quite intense reverse PT below p_ε^r.

There are two reasons for plastic flow under unloading. First, because of heterogeneous stress, strain, concentration, and, consequently, strength fields before unloading, reduction in the load leads to stress redistribution, during which stress intensity exceeds the yield strength in some regions. Then, in the regions with $p < p_\varepsilon^r$ (or $p > p_\varepsilon^d$), the reverse (or direct) PT starts. Volume change due to PTs under nonhydrostatic conditions causes additional plastic straining called transformation-induced plasticity (TRIP).[11,18,19] TRIP in turn leads to PTs thus serving as mechanochemical feedback.

Obtained results require reconsideration of the reported values of concentration in experiments,[24–29] which are based on the measurements of concentration after unloading. To avoid this problem for DAC, one can try to find loading, which will minimize reverse PT during unloading. Intuitively, utilization of a gasket with specially designed parameters that lead to quasi-homogenous pressure distribution during loading[19] should lead to minimization of plastic deformation and reverse PT during unloading. This case will be studied in the future.

V. PHASE TRANSFORMATIONS UNDER RELOADING

The aim of this section is to explore a new pressure-plastic strain path for strain-induced PTs by reloading sample after unloading to the same force. From Fig. 9, one can observe that with increase of load, first reverse PT propagates slowly, and direct PT does not occur until pressure is above p_ε^d. Further, in the pressure range $p_\varepsilon^r < p < p_\varepsilon^d$, direct PT starts to propagate along with reverse PT. When pressure reaches p_ε^r value, reverse PT cannot occur, and direct PT propagates through the sample with increased rate (Fig. 10, a, $F = 5.21$; and b, $F = 6.01$).

For a strong high pressure phase ($\sigma_{y2} = 5\sigma_{y1}$), PTs practically do not occur (similar to unloading), because the reloading occurs in the elastic regime due to high yield strength of the high pressure phase. For other cases, comparing the PTs before unloading in Fig. 6, direct PT is obviously less pronounced after unloading and reloading than during the first loading. In addition, reloading essentially changes the PT path and the PT region is more close to the center and plane of symmetry of a sample. For the case with $\sigma_{y2} = 0.2\sigma_{y1}$, after unloading and reloading, the thin PT band in Fig. 6 does not reappear and PT is not complete in the central region of a sample. For the case with $\sigma_{y2} = \sigma_{y1}$, while radius of the transformed zone is slightly increased, region with complete PT is slightly reduced.

Fig. 10 presents the distribution of accumulated plastic strain q, pressure p, and concentration of the high pressure phase c on the symmetry plane. At the initial stage of reloading, the strain is mostly elastic and an essential increase of plastic strain is only found at the higher force. Combination of low pressure and small increment in plastic strain, leads to practically unchanged concentration of the high pressure phase when dimensionless load F increases to 3.11. Further force growth results in pronounced growth in concentration

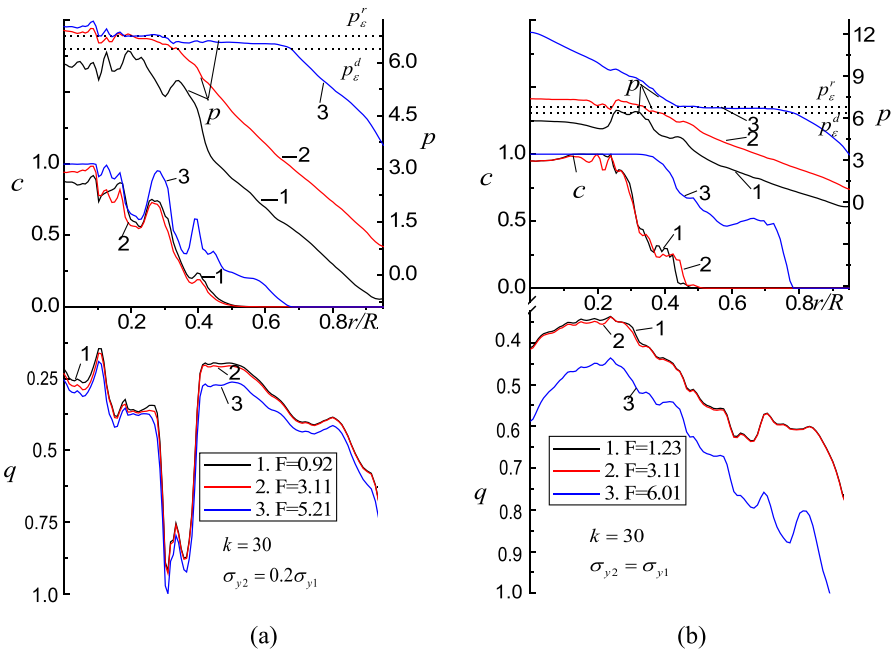

(a) (b)

FIG. 10. Distributions of accumulated plastic strain q, pressure p, and high pressure phase concentration c on symmetry plane under reloading, for $k = 30$ and $\sigma_{y2} \geq \sigma_{y1}$.

of the high pressure phase, especially in two-phase region. Larger two phase region leads to a wider plateau region, where pressure is between p^r_ε and p^d_ε. One can note that at initial reloading, due to low pressure, reverse PT instead of direct PT occurs in some regions. However, once the pressure in most regions is above p^d_ε, direct PT takes over and quickly propagates due to a relatively large accumulation of plastic strain. We also notice that the concentration of the high pressure phase in Fig. 10(b) slightly increases at $r \approx 0.43$ when load F increases to 3.11, despite the fact that the pressure is below p^d_ε. This occurs due to the flow of the high pressure phase toward the periphery rather than due to direct PT. Such a convective increase in concentration was not observed under first loading here and in previous papers.[13,21,22]

Fig. 11 shows the distribution of shear stress at contact surface under reloading. For the case with $\sigma_{y2} = 0.2\sigma_{y1}$, direct PT in the center of sample (Fig. 10(a)) results in the reduction of volume and flow of materials towards the center, which reduces the flow towards periphery due to recompression. Therefore, under reloading, shear stress in Fig. 11(a) gradually declines. However, for the case with $\sigma_{y2} = \sigma_{y1}$, the rate of direct PT in the two-phase region significantly surpasses that at the center (Fig. 10(b)), which caused flow of the material towards the two-phase region rather than the center of sample. Therefore, shear stress increases closer to the center due to recompression, and shear stress reduces in the two-phase region due to PTs. Comparing to the shear stress before unloading in Fig. 8, shear stress in a wide region significantly reduces after reloading.

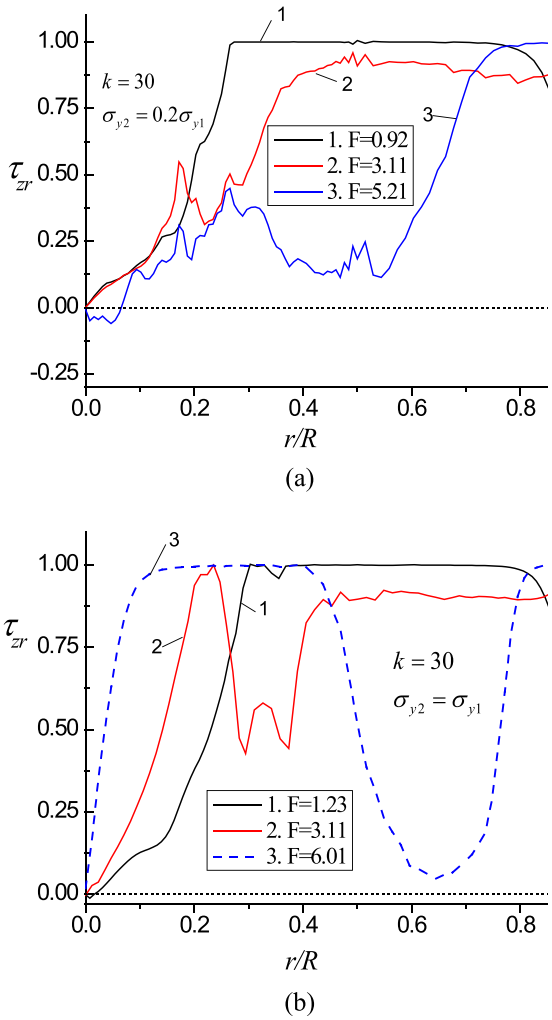

(a)

(b)

FIG. 11. Distribution of dimensionless shear stress τ_{zr} on contact surface under reloading, for $k = 30$ and $\sigma_{y2} \geq \sigma_{y1}$.

VI. CONCLUDING REMARKS

In this paper, strain-induced PTs in a sample in the DAC under loading, unloading, and reloading to the same force are investigated. A finite element approach and software

ABAQUS are utilized for solving a coupled system of equations for large plastic deformations and strain-induced PTs. In contrast to Ref. 22, where case $p_\varepsilon^d > p_\varepsilon^r$ was treated, here characteristic pressures satisfied the opposite inequality $p_\varepsilon^d < p_\varepsilon^r$ and values of p_ε^d and p_ε^rwere exchanged. PTs were studied for different kinetic parameters k and ratios of the yield strengths of high and low pressure phases. In general, under loading slightly more pronounced PT occurs for $p_\varepsilon^d < p_\varepsilon^r$ because of slightly lower p_ε^d. Geometry of the transformed zone is quite different for the case with $\sigma_{y2} = 0.2\sigma_{y1}$ that in Ref. 22. PT reaches the contact surface under smaller load, which is convenient for probing PTs by surface-based methods (e.g., Raman and optical methods) in experiments. However, extraction of the constants p_ε^d and p_ε^r from experimental pressure distribution is more problematic than for the case with $p_\varepsilon^d > p_\varepsilon^r$. Note that at the very initial stage of unloading, in the region where $p > p_\varepsilon^d$, a small increase in concentration (i.e., direct PT) is observed. Obtained pressure fields reproduce qualitative features observed in some experiments.

Under unloading, surprising plastic flow and extensive reverse PT are found for $\sigma_{y2} \leq \sigma_{y1}$, which were neglected in experiments. They are caused both by heterogeneous stress redistribution and TRIP. This PT requires reconsideration of quantitative values of phase concentrations in experiments on the unloaded sample, like in high pressure torsion[24,25] and ball milling.[26–29] The reverse PT may potentially be reduced or even avoided if a gasket with specially designed parameters will be used,[19] which creates quasi-homogenous pressure distribution under loading. This assumption will be checked in future studies. After reloading, the reverse PT continues followed by intense direct PT. However, PT is less pronounced than after initial compression to the same force and geometry of transformed zone changes. In particular, the localized transformed band of a weaker high pressure phase does not reappear in comparison with the initial compression. Also, an increase in concentration at a pressure below p_ε^d is observed, which occurs due to convective flow of the high pressure phase toward the periphery rather than due to direct PT. In the future, similar work will be performed for a sample under compression and torsion in rotational DAC. Since in majority of experiments devoted to study of strain-induced PTs in traditional DAC or rotational DAC[6–8,16,17,31] and high pressure torsion experiments,[23–25] there is no special gasket (i.e., the same material is used as the sample and gasket), we studied such a case here. However, to receive quasi-homogeneous pressure distribution, we recently introduced a gasket with specially determined parameters for strain-induced PTs as well.[18,19,38] We will study such a case numerically in the future.

ACKNOWLEDGMENTS

The support of Army Research Office (Grant No. W911NF-12-1-0340) managed by Dr. David Stepp, Defense Advanced Research Projects Agency (Grant W31P4Q-13-1-0010) managed by Dr. Judah Goldwasser, and Iowa State University was gratefully acknowledged.

[1]C. Nisr, G. Ribarik, T. Ungar, G. B. M. Vaughan, P. Cordier, and S. Merkel, J. Geophys. Res. **117**, B03201, doi:10.1029/2011JB008401 (2012).
[2]A. R. Oganov, J. H. Chen, C. Gatti, Y. Z. Ma, Y. M. Ma, C. W. Glass, Z. X. Liu, T. Yu, O. O. Kurakevych, and V. L. Solozhenko, Nature **457**, 863 (2009).
[3]T. S. Duffy, G. Y. Shen, D. L. Heinz, J. F. Shu, Y. Z. Ma, H. K. Mao, R. J. Hemley, and A. K. Singh, Phys. Rev. B **60**, 15063 (1999).
[4]A. Lazicki, P. Loubeyre, F. Occelli, R. J. Hemley, and M. Mezouar, Phys. Rev. B **85**, 054103 (2012).
[5]C. S. Zha, Z. X. Liu, and R. J. Hemley, Phys. Rev. Lett. **108**, 146402 (2012).
[6]V. V. Aksenenkov, V. D. Blank, N. F. Borovikov, V. G. Danilov, and K. I. Kozorezov, Dokl. Akad. Nauk **338**, 472 (1994).
[7]I. A. Barabanov, V. D. Blank, and Y. S. Konyaev, Instrum. Exp. Tech. **30**, 445 (1987).
[8]V. Blank *et al.*, Phys. Lett. A **188**, 281 (1994).
[9]C. Ji, V. I. Levitas, H. Zhu, J. Chaudhuri, A. Marathe, and Y. Ma, Proc. Natl. Acad. Sci. U.S.A. **109**, 19108 (2012).
[10]V. I. Levitas, Y. Z. Ma, E. Selvi, J. Z. Wu, and J. A. Patten, Phys. Rev. B **85**, 054114 (2012).
[11]V. I. Levitas, Phys. Rev. B **70**, 184118 (2004).
[12]V. I. Levitas and O. M. Zarechnyy, Phys. Rev. B **82**, 174123 (2010).
[13]V. I. Levitas and O. M. Zarechnyy, Phys. Rev. B **82**, 174124 (2010).
[14]V. I. Levitas, Europhys. Lett. **66**, 687 (2004).
[15]V. I. Levitas, Phys. Lett. A **327**, 180 (2004).
[16]V. D. Blank, Y. Y. Boguslavsky, M. I. Eremets, E. S. Itskevich, Y. S. Konyaev, A. M. Shirokov, and E. I. Estrin, Zh. Eksp. Teor. Fiz. **87**, 922 (1984).
[17]V. D. Blank and S. G. Buga, Instrum. Exp. Tech. **36**, 149 (1993).
[18]V. I. Levitas, Y. Z. Ma, and J. Hashemi, Appl. Phys. Lett. **86**, 071912 (2005).
[19]V. I. Levitas, Y. Z. Ma, J. Hashemi, M. Holtz, and N. Guven, J. Chem. Phys. **125**, 044507 (2006).
[20]H. K. Mao and P. M. Bell, Science **200**, 1145 (1978).
[21]V. I. Levitas and O. M. Zarechnyy, Europhys. Lett. **88**, 16004 (2009).
[22]O. M. Zarechnyy, V. I. Levitas, and Y. Z. Ma, J. Appl. Phys. **111**, 023518 (2012).
[23]M. T. Perez-Prado and A. P. Zhilyaev, Phys. Rev. Lett. **102**, 175504 (2009).
[24]K. Edalati, S. Toh, Y. Ikoma, and Z. Horita, Scr. Mater. **65**, 974 (2011).
[25]A. P. Zhilyaev, I. Sabirov, G. Gonzalez-Doncel, J. Molina-Aldareguia, B. Srinivasarao, and M. T. Perez-Prado, Mater. Sci. Eng., A **528**, 3496 (2011).
[26]F. Delogu, Scr. Mater. **67**, 340 (2012).
[27]F. Delogu, J. Mater. Sci. **47**, 4757 (2012).
[28]C. Suryanarayana, Rev. Adv. Mater. Sci. **18**, 203 (2008).
[29]L. Takacs, Prog. Mater. Sci. **47**, 355 (2002).
[30]V. I. Levitas, *Large Deformation of Materials with Complex Rheological Properties at Normal and High Pressure* (Nova Science, New York, 1996).
[31]N. V. Novikov, S. B. Polotnyak, L. K. Shvedov, and V. I. Levitas, J. Superhard Mater. **3**, 39 (1999).
[32]W. Kanitpanyacharoen, S. Merkel, L. Miyagi, P. Kaercher, C. N. Tome, Y. Wang, and H. R. Wenk, Acta Mater. **60**, 430 (2012).
[33]N. V. Novikov, V. I. Levitas, S. B. Polotnyak, and M. M. Potemkin, Strength Mater. **26**, 294 (1994).
[34]N. V. Novikov, V. I. Levitas, S. B. Polotnyak, and M. M. Potyomkin, High Pressure Res. **8**, 507 (1992).
[35]N. V. Novikov, V. I. Levitas, and S. B. Polotnyak, J. Superhard Mater. **9**, 1 (1987).
[36]ABAQUS V6.11. Abaqus User Subroutines Reference Manual: HETVAL and USDFLD. Providence RI, USA: Abaqus INC (2011).
[37]V. I. Levitas and O. M. Zarechnyy, J. Phys. Chem. B **110**, 16035 (2006).
[38]V. I. Levitas, J. Hashemi, and Y. Ma, Europhys. Lett. **68**, 550 (2004).